Transmission electron microscopy on live catalysts

Bremmer, G.M.

CHAPTER 2

Instability of $NiMoS_2$ and $CoMoS_2$ hydrodesulfurization catalysts at ambient conditions: A quasi *in situ* High-Resolution Transmission Electron Microscopy and X-Ray Photoelectron Spectroscopy study

The effect of exposure to ambient air of MoS_2-based, γ-Al_2O_3-supported HDS catalysts has been studied using HRTEM. Analysis of unpromoted as well as Ni- and Co-promoted MoS_2 samples showed that the number of MoS_2 slabs and the average slab length decreased as a function of air exposure time. A parallel XPS study showed this effect to be due to oxidation. During the first 24 h of exposure to air, all 1 bar sulfided (Ni/Co)MoS_2 samples showed an initial slab length decrease of around 20%. After an additional month in air, the slabs had deteriorated significantly further. A sample of $CoMoS_2$, sulfided at 30 bar, showed a slightly enhanced effect of oxidation, particularly after the first 5 minutes in air. The data obtained in this study emphasize the general necessity of shielding vulnerable catalyst samples from air during preparation and characterization, a message relevant in all fields of research covering catalysis.

2.1 Introduction

Current environmental legislation pushes oil refiners toward producing transportation fuels with progressively lower sulfur levels in order to limit the emission of harmful sulfur-containing exhaust gases into the atmosphere.[1] The main reaction used to remove organosulfur compounds from oil feedstock is the catalytic hydrodesulfurization (HDS) reaction. The industrial HDS catalysts used most for this purpose are based on MoS_2, present in the form of nanometer-sized slabs dispersed on a high-surface-area support, such as γ-Al_2O_3.[2] MoS_2 catalyst slabs consist of one layer of molybdenum atoms sandwiched between two layers of sulfur atoms.[2-4] MoS_2 is also being studied as a material with interesting electrical properties (e.g., to be used as a semiconductor material in nanoelectonics [5-8]. It has applications in photocatalysis,[9,10] and MoS_2 is used as a solid lubricant. [11-13] Research on MoS_2 has been a long ongoing effort, in which a wide variety of characterization techniques have been used. In 2008, Kooyman and van Veen reported the importance of shielding γ-Al_2O_3-supported MoS_2 catalysts from ambient air between preparation and characterization.[14] Their transmission electron microscopy (TEM) study indicated that exposing MoS_2 samples to ambient air leads to deterioration of the catalyst slabs, but no mechanism for this phenomenon was proposed.

Promoting MoS_2-slabs with metal atoms such as nickel or cobalt has the effect of enhancing the catalytic activity of the catalyst, as well as influencing the specific selectivity.[15-17] The influence of the incorporated promoter atoms on the stability of the catalyst slabs has not yet been studied. The effect of the promoter atoms could be stabilizing, causing the slabs not to deteriorate because of mere exposure to ambient conditions, but the effect might also cause less stability in air, as the promoted catalyst slabs are more reactive in general because of the presence of more coordinatively unsaturated sites.

We have investigated this issue by using quasi *in situ* high-resolution transmission electron microscopy (HRTEM) to monitor the effect of ambient air on $NiMoS_2$, $CoMoS_2$, and MoS_2 samples sulfided at 1 bar. After preparation of the samples, special care was taken to prevent contact with air during transportation and prior to the TEM imaging. We determined the average length and stacking of the catalyst slabs for each sample after the first TEM measurements, without contact with ambient air, as well as after 24 h and after 1 month of air exposure. Because many industrial processes using these catalysts are operated at high pressures (30-100 bar), a Co-promoted MoS_2-catalyst was sulfided at 30 bar for comparison. A parallel quasi *in situ* X-ray photoelectron spectroscopy (XPS) study was performed to monitor the chemical changes of the catalyst, following the same approach of air exposure.

2.2 Experimental

2.2.1 Preparation of catalysts

The four catalyst samples were prepared by incipient-wetness coimpregnation of Ketjen CK-300 γ-Al_2O_3 extrudates (SBET = 250 m^2/g, Vpore = 0.66 mL/g), which were crushed and sieved to a 125-250 μm fraction prior to impregnation. Different aqueous solutions containing cobalt(II) nitrate ($Co(NO_3)_2 \cdot 6H_2O$, Merck), nickel-

(II) nitrate ($Ni(NO_3)_2 \cdot 6H_2O$, Merck), ammonium heptamolybdate ($(NH_4)_6Mo_7O_{24} \cdot 4H_2O$, Merck), and nitrilotriacetic acid (NTA, $(C_2H_3O_2)_3N$, Merck) were prepared to obtain catalysts with 8 wt % Mo and 1.5 wt % Co or Ni for the promoted catalysts. The molar ratio of NTA:Mo was 1.2:1. All catalyst precursors were dried at room temperature for 1 h, dried in static air at 100 °C overnight, and finally calcined at 450 °C (heating rate, 6 °C/min) in flowing air for 4 h. The catalyst precursors were sulfided at 350 °C (heating rate, 6 °C/ min) for 2 h in H_2/H_2S 9:1 (Scott), in a flow of 60 mL/min STP at a total pressure of 1 or 30 bar. The samples sulfided at 1 bar are termed $NiMoS_2$, $CoMoS_2$, and MoS_2, while the Co-promoted sample sulfided at 30 bar is termed $CoMoS_2$-30. After preparation, each sample was collected in a glass vial, which was filled with N_2 and sealed airtight for transportation.

2.2.2 Exposure to ambient air

The vials containing the sulfidic catalysts were opened in an Ar-filled glovebox (concentrations of H_2O and O_2 < 1 ppm), after which the samples were mounted on TEM grids as described below. After the first quasi *in situ* TEM study of the samples, without any exposure to air, the samples on the TEM grids were left on an office desk in a small nonairtight plastic box, to prevent accumulation of dust but to allow exposure to ambient air. This procedure is very similar to the storage of larger samples of catalyst in containers on a shelf and is different from passivation. For passivation, a material is first exposed to a low, controlled, concentration of oxygen *before* being exposed to ambient air. For many materials this creates a protective oxide layer that prevents further oxidation and can be removed by mild reduction.

2.2.3 Characterization of catalysts

Quasi *in situ* TEM was carried out using an FEI monochromated Tecnai F20ST/ STEM electron microscope, operated at an accelerating voltage of 200 keV, in bright field TEM mode. Images were obtained using a Gatan Ultrascan CCD camera (4k × 4k).

The vials containing the prepared samples were opened in an Ar-filled glovebox (concentrations of H_2O and O_2 < 1 ppm), after which the samples were crushed in *n*-hexane using a mortar and pestle, creating a suspension. A few drops of the suspension were placed on a Quantifoil microgrid carbon-film covered mixed mesh Au TEM grid and, after evaporation of the solvent at room temperature, the grid was placed in a protective atmosphere transfer TEM specimen holder.[18] This holder was inserted into the glovebox via an air-lock. The holder was then closed (the sample compartment is sealed by a Viton O-ring), removed from the glovebox air-lock, and transferred to the TEM for imaging. Once the holder was inserted in the TEM air-lock, one 3 min pumping cycle was started while the holder was still closed, and the sample compartment of the holder was opened at the beginning of a second 3 min pumping cycle.

Samples were imaged quasi *in situ* (t = 0, without exposure to air), after 24 h of exposure to air (t = 24 h), and after 1 month in air (t = 1 month). The $CoMoS_2$-30 sample was also imaged after 5 min in air (t = 5 min). The average slab length of each sample was determined for quantitative analysis. Qualitative analysis was made possible by imaging identical regions of the samples at the different points in time.

To investigate possible effects of the high-energy electron beam on the sample, also control images of sample regions that had not been exposed to the electron beam before were recorded and analyzed.

The resulting images were analyzed using Gatan Digital Micrograph and ImageJ software. After the slabs were identified, the length of each slab was measured by hand using standard drawing tools in the software. Per sample, around 800 individual slabs were measured at $t = 0$. Due to the detrimental effect of ambient air on the slabs, at $t = 24$ h about 450 slabs per sample were left for analysis, while after 1 month in air only around 300 slabs were left for analysis in the same regions of the samples that had been studied before.

The same samples were analyzed with XPS using a Kratos AXIS Ultra spectrometer, equipped with a monochromatic X-ray source and a delay-line detector (DLD). To prevent contact with air, samples were transferred from the glovebox to the XPS in a closed, homemade transfer holder under N_2 atmosphere. Spectra were recorded using an aluminum anode (Al Kα = 1486.6 eV). Survey scans were measured at constant pass energy of 160 eV and region scans at 40 eV. The background pressure was 2×10^{-9} mbar.

XP spectra were fitted with CasaXPS (version 2.3.16) by a nonlinear least-squares fitting algorithm using mixed Gaussian-Lorentzian (35/65) curves. Shirley background subtraction was applied, and the energy was calibrated using the Al 2p peak at 74.6 eV as a reference. The Mo 3d spectrum was fitted with Mo^{4+} (MoS_2), Mo^{5+} (MoS_xO_y), and Mo^{6+} (MoO_3) contributions, as well as with the overlapping S 2s (~226.5 eV) component. The Ni 2p and Co 2p spectra were fitted with a sulfidic M^{2+} contribution and an oxidic M^{2+} contribution (NiO, CoO). The sulfidic contribution was assigned to Ni or Co sulfides, either dispersed on the edges of MoS_2 particles or present as bulk metal sulfides (Ni_3S_2, Co_9S_8). Lastly, the S^{2-} and bridged S_2^{2-} anions, as well as sulfate (SO_4^{2-}), were taken into account for fitting the S 2p spectra. The XPS fitting procedure is explained in more detail in a recent paper.[19] The respective binding energies of these components are listed in Table 2.1 and agree well with previously reported studies.[20-22]

Table 2.1. XPS Binding energies of the various species present in (Co/Ni)MoS_2, as determined by the fitting procedure described in the text.

	Mo^{4+} (MoS_2)	Mo^{5+} (MoS_xO_y)	Mo^{6+} (MoO_3)	S^{2-} (MS_x)	S_2^{2-} (MS_x)
BE (eV)[a]	229.0	231.2	232.7	161.7	163.2
ΔBE (eV)[b]	3.15	3.15	3.15	1.15	1.15
	S^{6+} (SO_4^{2-})	Co^{2+} (CoS_x)[c]	Co^{2+} (CoO)[c]	Ni^{2+} (NiS_x)[c]	Ni^{2+} (NiO)[c]
BE (eV)[a]	168.8	778.7	791.8	853.8	856.5
ΔBE (eV)[b]	1.15	-	-	-	-

[a] Binding energy of the $3d_{5/2}$ or $2p_{3/2}$ peak. Uncertainty ± 0.2 eV.
[b] $\Delta BE(3d) = BE(3d_{3/2}) - BE(3d_{5/2})$; $\Delta BE(2p) = BE(2p_{1/2}) - BE(2p_{3/2})$.
[c] Only the $2p_{3/2}$ peak was fitted for Co and Ni.

2.3 Results and discussion

2.3.1 Imaging and slab length analysis

A set of representative TEM images of the $NiMoS_2$ sample is shown in Figure 2.1, where the same γ-Al_2O_3 particle covered with $NiMoS_2$ slabs was imaged before any exposure to air, after 24 h in air, and after 1 month of exposure to air. It is immediately apparent that exposure to air leads to a decrease in the total number of visible slabs. For example, the slab that is indicated in the encircled region labeled "1" is present at $t = 0$ but has disappeared at $t = 24$ h. There are several other slabs that are present in the first image but are no longer visible after the sample has been exposed to ambient air. The second indication that the sample was affected by air is that the observed average length of the slabs is decreasing. The stack of multiple slabs in the encircled region labeled "2" is an example of this phenomenon. At $t = 0$, the stack consists of three slabs of approximately equal length. The length of the slabs decreases significantly upon exposure to air. It can also be noted that the substrate that carries the slabs seems to be changing simultaneously. Although this is not clearly visible in TEM imaging, the substrate material that supports the visible slabs does not consist solely of γ-Al_2O_3. It is actually γ-Al_2O_3 covered with more $NiMoS_2$ slabs that are oriented nonparallel with respect to the TEM electron beam and thus not clearly visible as slabs. Due to the planar layered structure of MoS_2, the only slabs that will be visible in the TEM two-dimensional projection are those that are oriented parallel, or slightly tilted (± several degrees) with respect to the electron beam.[23] As all $NiMoS_2$ slabs are influenced by ambient air, also the slabs that are not directly visible are changing. The result of this process is observed as changes in general morphology of the material surrounding and supporting the visible slabs, which is for example visible when comparing the edge structure of the particle in Figure 2.1 at the different stages of oxidation.

For the $CoMoS_2$, $CoMoS_2$-30, and MoS_2 samples, similar trends are found, with less and apparently shorter slabs being observed. All samples show slabs decreasing both in length as well as in number after exposure to air.

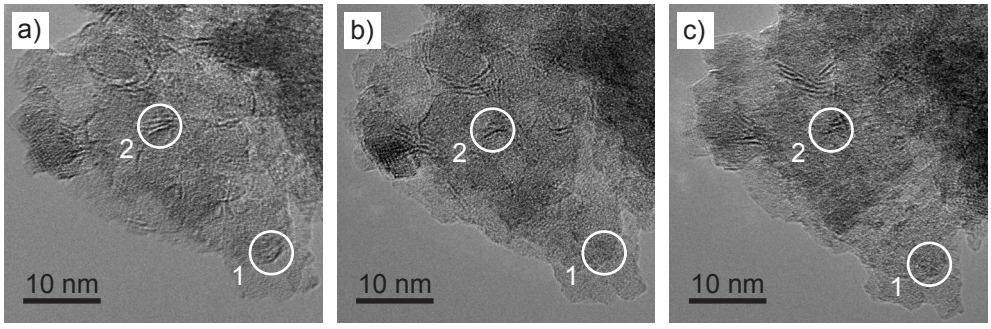

Figure 2.1. TEM images of a γ-Al_2O_3 particle covered with $NiMoS_2$ catalyst slabs: (a) prior to air exposure, (b) after 24 h of exposure to air, and (c) after 1 month in ambient air. Several catalyst slabs have disappeared after air exposure. The region labeled "1" shows a slab that has completely disappeared after 24 h of air exposure, while the region labeled "2" shows a stack of which the slabs have become shorter over time.

However, solely based on observations of a small number of slabs, no conclusions can be drawn. As the sample grid is taken out of the sample holder between the measurements, it might occur that a slab that was visible in the t = 0 measurement is no longer visible during the t = 24 h or t = 1 month measurement because of a slight rotation of a part of the material. The opposite process might also occur, resulting in slabs appearing that were not visible before. Therefore, quantitative slab length analysis based on a large set of images is required. In this way, the random process of slabs appearing or disappearing due to changes in carrier material and observation angle will be averaged out.

For statistical analysis of the changes of the samples upon contact with air, all recorded images were analyzed and the lengths of all visible slabs were measured. For the $NiMoS_2$ sample, the t = 0 measurement yielded 761 measured slabs, while the images of the same areas of the sample obtained after 24 h of air exposure showed 631 slabs for analysis. After 1 month in air, 585 slabs remained visible. The distribution of the recorded slab lengths is plotted as a histogram in Figure 2.2a.

The slab length distribution changes significantly after exposure to air. At t = 0, the slab length distribution is more evenly distributed over slab lengths between 1 and 3 nm, with a long tail stretching to 4.5 nm. At t = 24 h, the distribution of the histogram has mostly shifted to the regime between 1 and 2 nm, with a peak around 1.3 nm. This process continues during the 1 month of exposure to air, as is visible in the t = 1 month histogram. The number of slabs shorter than 1 nm has increased significantly, while the tail of the histogram decreases further. As the slabs get shorter, slabs that were initially relatively short (< 1 nm) disappear completely, explaining the decrease in the total number of observable slabs. The stacking degree of the slabs was also determined, resulting in an average stacking of 1.3 layers, which remained constant after exposure to air. Analysis of the other samples was performed in the same way, resulting in the histograms shown in Figure 2.2b-d. All samples show similar trends in slab length distribution, indicating that all samples are affected by exposure to air in a similar way, including the reference sample of unpromoted MoS_2 (Figure 2.2c).

When $CoMoS_2$ and $CoMoS_2$-30 bar are compared, some differences are visible. The initial slab length distribution at t = 0 shows a broader distribution for the 30 bar sulfided sample. At t = 5 min, a shift is already visible in the distribution of the histogram, which indicates that only 5 min of exposure to air has an effect on the slabs. The distribution continues to shift after extended exposure to air. The calculated average slab lengths are shown in Table 2.2. Although $CoMoS_2$-30 initially has a slightly higher average slab length value than the 1 bar sulfided $CoMoS_2$ sample, after exposure to air for 1 month the average slab lengths of both samples have decreased to similar values. The average slab length of $CoMoS_2$-30 decreased faster than that of $CoMoS_2$. The average slab stacking degree was also determined for each sample, yielding similar values for all samples: around 1.3 ± 0.1 layers per cluster. These values remained constant during air exposure.

When the average slab length values per sample as a function of air exposure time is plotted, it is clear that all samples were affected (Figure 2.3). All samples showed a significant decrease in average slab length. Average slab length values were also determined from control images, obtained from areas that had not been exposed to the TEM electron beam before. The data are shown in Table 2.2. The t = 0 measurements did not require control data, because for these data the sample was

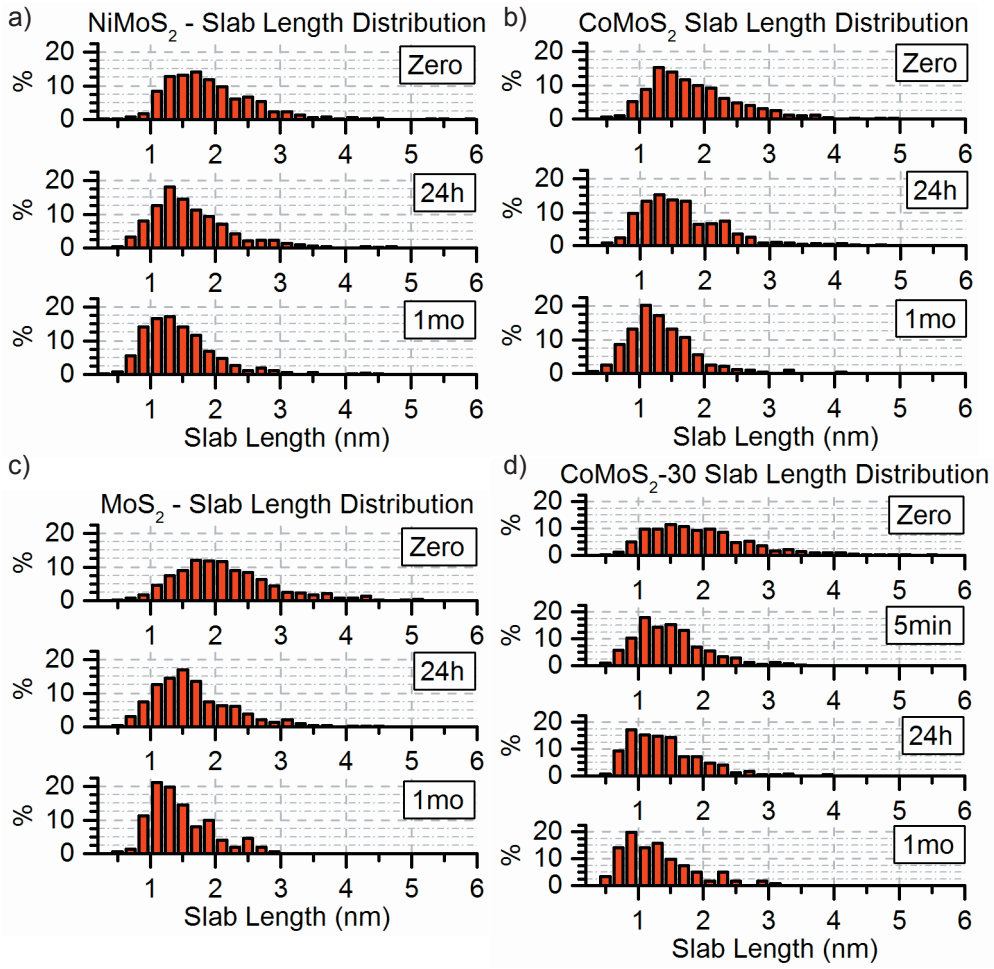

Figure 2.2. Sets of histograms showing the slab length distribution of: (a) $NiMoS_2$, (b) $CoMoS_2$, (c) MoS_2, and (d) $CoMoS_2$-30, as a function of air exposure time.

Table 2.2. Average Slab Length (l) in nm of each sample, including the control data of parts of the sample that had not previously been exposed to the electron beam.

	$NiMoS_2$	$CoMoS_2$	$CoMoS_2$-30	MoS_2
Zero	1.91	1.83	1.98	2.16
5 min in air			1.48	
24 h in air	1.65	1.64	1.39	1.66
Control 24 h	1.80	1.76	1.55	1.78
1 month in air	1.45	1.33	1.29	1.46
Control 1 month	-	1.52	1.37	1.76

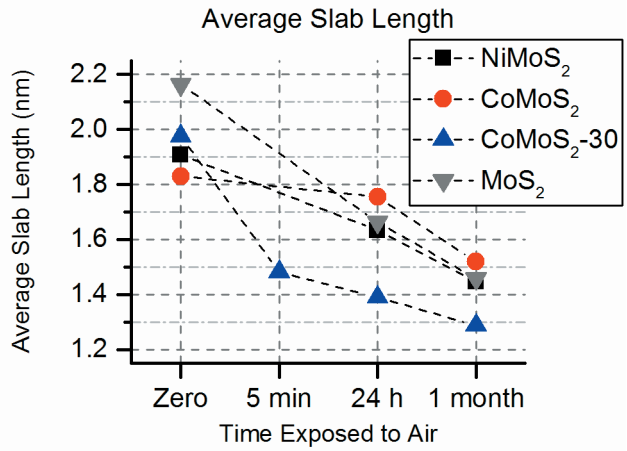

Figure 2.3. Average slab length of all (Ni/Co)MoS_2 samples as a function of air exposure time.

exposed to the electron beam for the first time. Although $NiMoS_2$ t = 24 h control data were inadvertently not obtained, the data show a clear trend. Slabs in areas that had not yet been exposed to the electron beam also decreased in length, but at a somewhat lower rate. This indicates that exposure to the electron beam had a minor accelerating contribution to the process of slab deterioration.

2.3.2 X-ray Photoelectron Spectroscopy

To obtain detailed information concerning the composition of the catalyst at the different stages of air exposure during the experiments, we performed X-ray photo- electron spectroscopy. Figure 2.4 shows the acquired XP spectra of the catalyst samples, demonstrating the change in atomic composition as a function of air exposure time. At t = 0, approximately 80% of Mo and Ni and 90% of Co was present as the respective metal sulfides. All sulfur was present as sulfidic sulfur (S^{2-}, S_2^{2-}). For $CoMoS_2$, sulfidation at 30 bar slightly increased the fractions of MoS_2 and Co sulfide compared with sulfidation at 1 bar. Upon brief exposure to air (5 min), no oxidation of Mo or S was apparent in the XP spectra, whereas slight oxidation (approximately 10%) of the Ni/Co promoter atoms could be observed after deconvolution of the XP spectra in the promoted catalysts. After an additional 24 h of exposure to air, approximately 15% of Mo, 6% of S, 39% of Ni, and 24% of Co was oxidized compared with the freshly sulfided catalysts at t = 0. Oxidation of the Mo and S species occurred at approximately the same rates in both the promoted and unpromoted samples. The promoted catalysts were most prone to oxidation as the Ni and Co atoms oxidized first. The oxidation of Co leveled off after 24 h of exposure to air, whereas Ni oxidation was an ongoing process.

After 1 month of exposure to air, all catalysts showed significant oxidation of all elements. Even sulfur, which oxidized more slowly than the other elements, was significantly oxidized after 1 month of exposure to air. The observed sequence of oxidation over time was Ni/Co > Mo > S. The data depicted in Figure 2.4 are listed in Table 2.2.

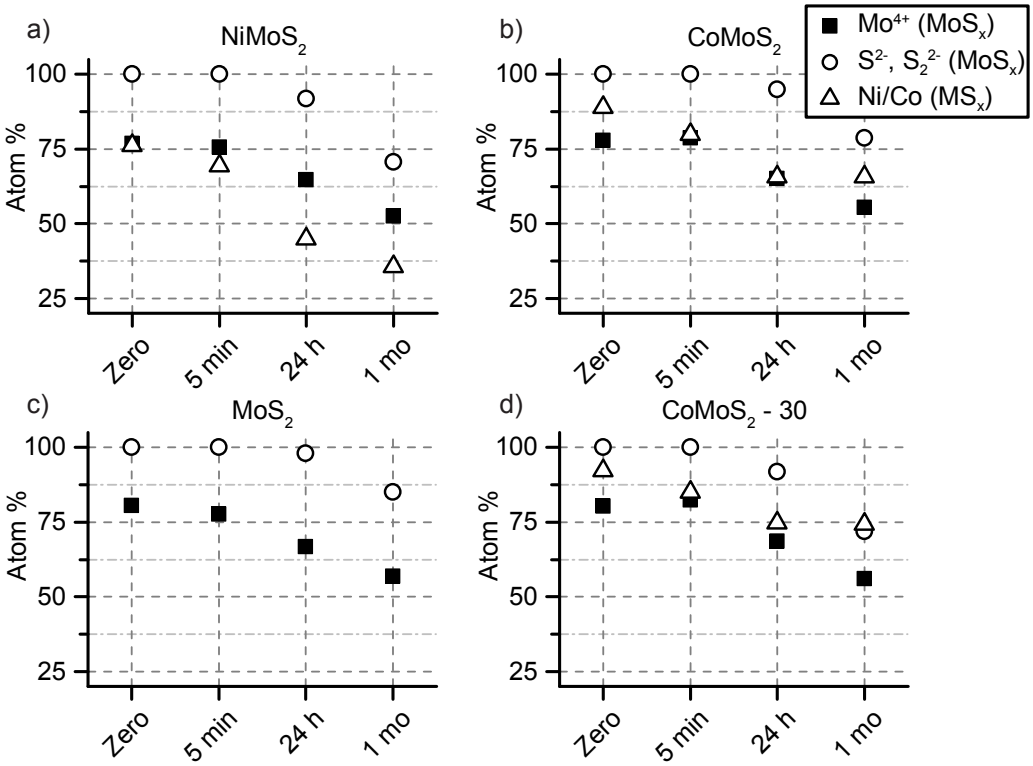

Figure 2.4. Composition (in atom %, as determined by deconvolution of XP spectra) of the samples (a) $NiMoS_2$,(b) $CoMoS_2$, (c) MoS_2, and (d) $CoMoS_2$-30, prior to exposure to air and after 5 min, after 24 h, and after 1 month of exposure to air. The fraction of sulfided species was calculated from the contributions of MoS_2 (Mo^{4+}), sulfide anions (S^{2-} and S_2^{2-}) and sulfided Ni/Co (either as M-MoS_2 or as MS_x).

The Ni 2p, Mo 3d, and S 2p XP spectra of $NiMoS_2$ are plotted in Figure 2.5 and are representative for all catalysts exposed to air. The XP spectra for the other samples are shown in Figures 2.6 - 2.8. Oxidation of the MoS_2-phase was evident from the appearance of a peak at 235.9 eV in Figure 2.5b, which can be ascribed to Mo^{6+}, as in MoO_3 ($3d_{3/2}$). The formation of NiO was shown by the peak at 856.5 eV appearing in the Ni 2p spectrum (Figure 2.5a) as well as by the appearance of satellite features at ~862 eV (Ni $2p_{3/2}$) and ~880 eV (Ni $2p_{1/2}$). In agreement with these observations, a peak at 168.8 eV appeared in the S 2p spectrum (Figure 2.5c), indicative of the formation of sulfates. After 1 month of exposure to air, increased oxidation was observed in all spectra.

Table 2.2. Composition (atom %, as determined by deconvolution of XP spectra) of the samples $NiMoS_2$, $CoMoS_2$, MoS_2, and $CoMoS_2$–30, prior to exposure to air, after 5 minutes, after 24 hours, and after 1 month of exposure to air. The fraction of sulfided species was calculated from the contributions of MoS_2 (Mo^{4+}), sulfide anions (S^{2-} and S_2^{2-}) and sulfided Ni/Co (either as M-MoS_2 or as MS_x) to the respective XP spectra.

	$NiMoS_2$			**$CoMoS_2$**		
	Mo^{4+}	S^{2-}, S_2^{2-}	Ni	Mo^{4+}	S^{2-}, S_2^{2-}	Co
Zero	76.8	100.0	76.2	77.8	100.0	89.0
5 min	75.6	100.0	69.5	78.6	100.0	79.9
24 h	64.7	91.8	44.9	65.1	95.0	65.6
1 month	52.5	70.6	35.7	55.4	78.7	65.7
	MoS_2			**$CoMoS_2$ - 30**		
	Mo^{4+}	S^{2-}, S_2^{2-}		Mo^{4+}	S^{2-}, S_2^{2-}	Co
Zero	80.5	100.0		80.3	100.0	92.3
5 min	77.7	100.0		82.3	100.0	85.0
24 h	66.6	97.9		68.6	91.9	74.8
1 month	56.8	85.0		55.9	71.9	74.3

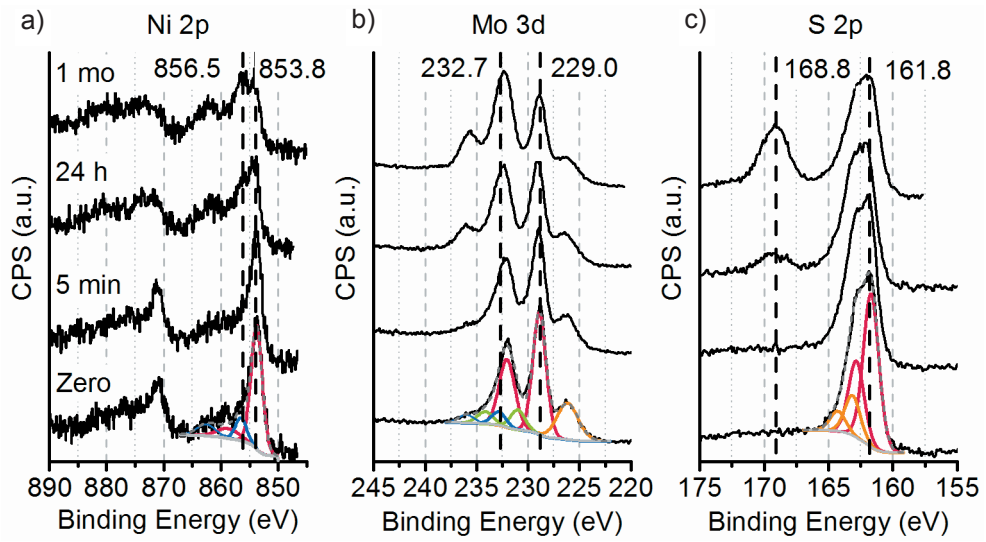

Figure 2.5. XP spectra of $NiMoS_2$, showing the (a) Ni 2p, (b) Mo 3d, and (c) S 2p signals, prior to exposure to air and after 5 min, 24 h, and 1 month of exposure to air. The binding energies (BE) of sulfided species (lower BE) and oxidized species (higher BE) are indicated by the dotted lines. The deconvolution is also shown. (a) Ni 2p: NiS_x, red; NiO_x, blue (both include satellites). (b) Mo 3d: Mo^{4+}, red; Mo^{5+}, green; Mo^{6+}, blue; for S 2s, orange. (c) S 2p: S^{2-}, red; S_2^{2-}, orange. In all graphs: background, light gray; fit, gray dashed; data is black.

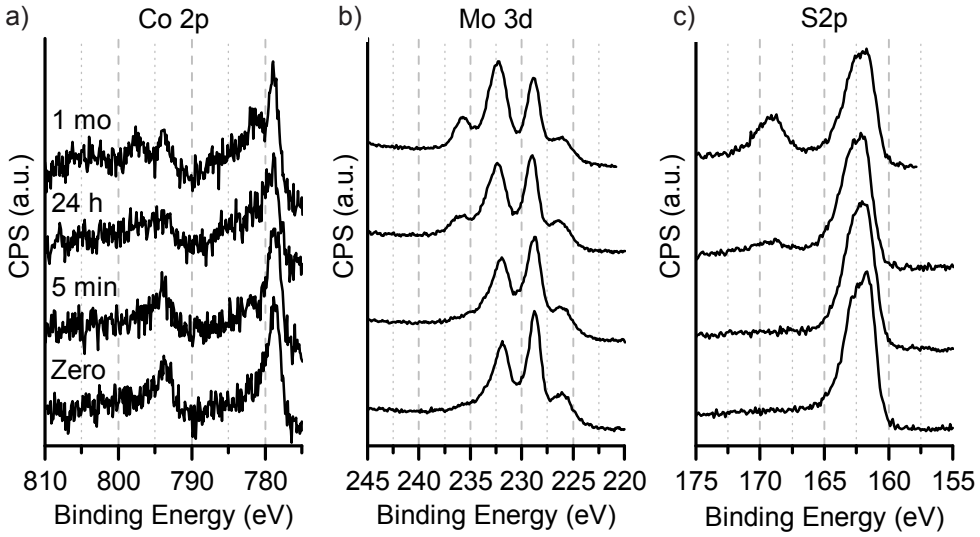

Figure 2.6. XP spectra of $CoMoS_2$, showing (a) the Co 2p, (b) the Mo 3d, and (c) the S 2p signals, prior to exposure to air, after 5 minutes, 24 h, and 1 month of exposure to air.

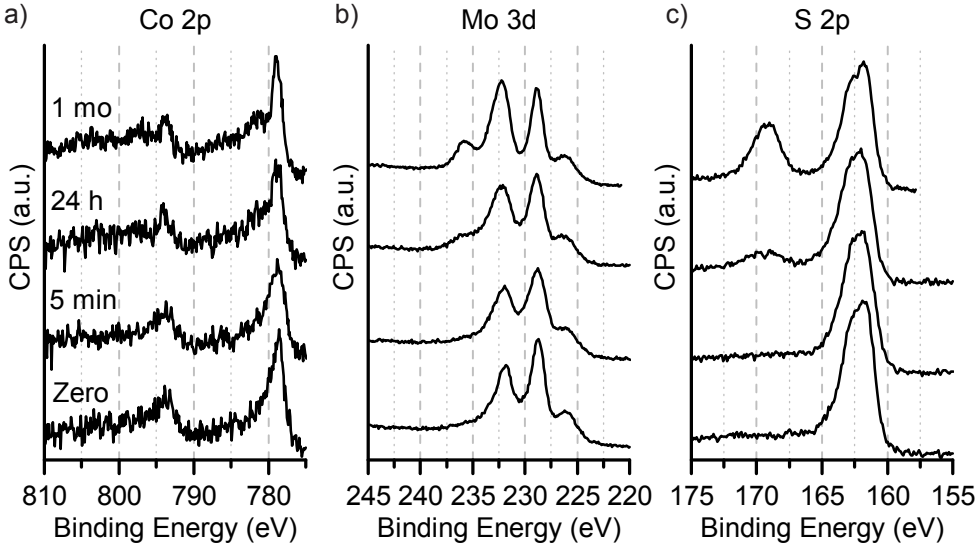

Figure 2.7. XP spectra of $CoMoS_2$-30, showing (a) the Co 2p, (b) the Mo 3d, and (c) the S 2p signals, prior to exposure to air, after 5 minutes, 24 h, and 1 month of exposure to air.

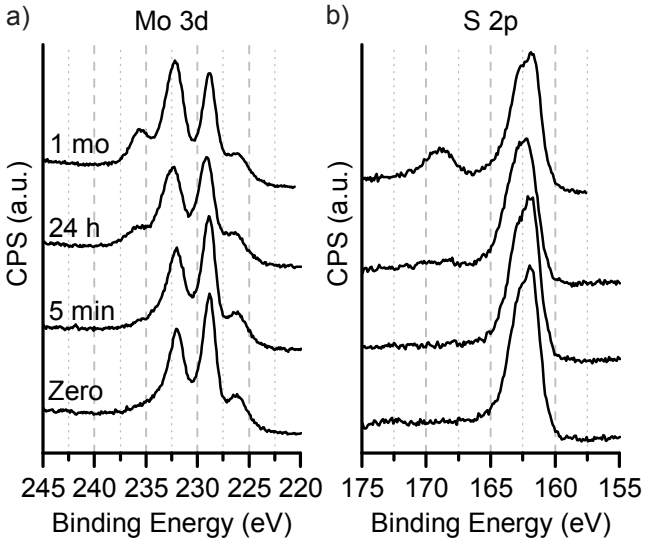

Figure 2.8. XP spectra of MoS_2, showing (a) the Mo 3d, and (b) the S 2p signals, prior to exposure to air, after 5 minutes, 24 h, and 1 month of exposure to air.

2.3.3 Proposed oxidation mechanism.

On the basis of the obtained TEM data alone, it is not easy to go beyond the slab-length analysis presented above and draw additional conclusions, e.g., about the atomic structure, location, and orientation of the new species that were formed during exposure to air. Combining the TEM observations with the XP spectra, we can, however, draw further conclusions.

Exposure to air leads to oxidation of the samples, as is indicated by the XP spectra shown in Figures 2.4 and 2.5. The oxidation initiates at the Ni/Co promoter atoms and continues with the oxidation of Mo after prolonged exposure to air. As is visible in the TEM micrographs, the slabs disappear from the sides of the particle toward the center. In various other studies, it has been shown that MoS_2-catalyzed reactions occur on the edges of the MoS_2 crystals, supported on a variety of materials.[4,24-28] The catalytically active species are the metal atoms located at the edges of the slabs. The oxide species that are formed there (MoO_3, oxysulfides) have no planar crystal structure;[14,23] hence, the edges of the slabs disappear in the TEM images, enabling us to observe a change in slab length.

The suggestion that oxidation of the slabs starts from the edge is also supported by the XPS data, which show the initial oxidation, during the first 5 min of exposure to air, to occur at the Ni/Co promoter atoms, to form NiO_x/CoO_x. However, this is not conclusive on its own because it has not been indisputably shown that the promoter atoms in (Ni/Co)MoS_2, supported on γ-Al_2O_3, are located on the edges of the MoS_2 slabs, as was shown in various other studies of (Ni/Co)MoS_2 on different supports (e.g., Au single-crystal surfaces or graphite).[29-32] Also, the initial Ni/Co oxidation XPS signal could, at least partially, originate from the oxidation of Ni/Co atoms that were not incorporated in the (Ni/Co)MoS_2 slabs but were contained in other species on the sample, such as Ni/Co-sulfides.[30] This suggestion is also

supported by the fact that γ-Al_2O_3-supported Co-sulfides oxidize more readily than γ-Al_2O_3-supported MoS_2.[33]

The scale of the horizontal axes in the graphs that show the evolution of the samples as a function of air exposure time is close to logarithmic (Figures 2.3 and 2.4). The approximately linear curves in these plots indicate an exponential decrease in average slab length. On average, during the first 24 h of air exposure, the average slab length of all samples decreased by 20%. After one more month in air, the decrease had continued up to an average decrease of 30%. As the oxidation rate was initially high but then exponentially slowed, the process appeared to be self-limiting. This could indicate that when the edges of the (Ni/Co)MoS_2-slabs were oxidized, the formed oxide species remained at the support around the slab, thereby shielding the inner MoS_2-species from oxidative attacks by incoming oxygen molecules, as was proposed by Yoshimura *et al*. in 1991.[33] As the basal planes of the slabs are known to be inactive,[34,35] the oxide ring would be formed only at the edges. When this oxide ring around the slab grew thicker, further oxidation of the remaining slab occurred at a progressively lower rate. This mechanism also explains the slightly accelerating effect of the electron beam on the oxidation process, given in Table 2.2.

The accelerating effect could be due to the fact that the beam might be able to (slowly) partly disintegrate the protective ring, allowing further oxidation to occur on the slabs that have been imaged multiple times. To prove this hypothesis, additional measurements would be required, however (e.g., using scanning transmission electron microscopy or scanning tunneling microscopy on flat model systems to localize and visualize the formed oxide species). This hypothesis also explains why the method of oxygen titration/chemisorption does not give quantitative results for the number of active sites:[36] the sites are being changed by the adsorbed oxygen.

2.4 Conclusion

Ni/Co-promoted and unpromoted MoS_2 catalyst particles, dispersed on a γ-Al_2O_3 substrate, are not stable in ambient air. TEM imaging reveals that on average the length of the (Ni/Co)MoS_2-slabs decreases as a function of air exposure time. Even 5 min of exposure to ambient air already significantly decreases the average slab length. XPS shows that the samples are being oxidized. Oxidation of the catalyst slabs occurs from the edges toward the center of the slab, after which the formed oxide species probably remain around the slab. These remaining oxide species might form a ring-like barrier structure around the inner MoS_2-species, shielding these inner species from oxidation and explaining the exponential decay of the process.

References

[1] Environmental Protection Agency. Control of Air Pollution From Motor Vehicles: Tier 3 Motor Vehicle Emission and Fuel Standards; Final Rule; **2014**, Vol. 79.

[2] Eijsbouts, S.; Heinerman, J.; Elzerman, H. MoS_2 Structures in High-Activity Hydrotreating Catalysts. *Appl. Catal. A* **1993**, *105* (1), 53–68 DOI: 10.1016/0926-860X(93)85133-A.

[3] Füchtbauer, H. G.; Kibsgaard, J.; Lauritsen, J. V.; Tuxen, A. K.; Lægsgaard, E.; Li, Z.; Clausen, B. S.; Topsøe, H.; Besenbacher, F. Morphology and Atomic-Scale Structure of MoS_2 Nanoclusters Synthesized with Different Sulfiding Agents. *Top. Catal.* **2013**, *57* (1-4), 207–214 DOI: 10.1007/s11244-013-0176-1.

[4] Lauritsen, J. V.; Nyberg, M.; Nørskov, J. K.; Clausen, B. S.; Topsøe, H.; Lægsgaard, E.; Besenbacher, F. Hydrodesulfurization Reaction Pathways on MoS_2 Nanoclusters Revealed by Scanning Tunneling Microscopy. *J. Catal.* **2004**, *224* (1), 94–106 DOI: 10.1016/j.jcat.2004.02.009.

[5] McGovern, I. T.; Dietz, E.; Rotermund, H. H.; Bradshaw, A. M.; Braun, W.; Radlik, W.; McGilp, J. F. Soft X-Ray Photoemission Spectroscopy of Metal-Molybdenum Bisulphide Interfaces. *Surf. Sci.* **1985**, *152-153*, 1203–1212 DOI: 10.1016/0039-6028(85)90540-0.

[6] Wilcoxon, J.; Samara, G. Strong Quantum-Size Effects in a Layered Semiconductor: MoS_2 Nanoclusters. *Phys. Rev. B* **1995**, *51* (11), 7299–7302 DOI: 10.1103/PhysRevB.51.7299.

[7] Mak, K. F.; Lee, C.; Hone, J.; Shan, J.; Heinz, T. F. Atomically Thin MoS_2: A New Direct-Gap Semiconductor. *Phys. Rev. Lett.* **2010**, *105* (13), 136805 DOI: 10.1103/PhysRevLett.105.136805.

[8] Yazyev, O. V.; Kis, A. MoS_2 And Semiconductors in the Flatland. *Mater. Today* **2015**, *18* (1), 20–30 DOI: 10.1016/j.mattod.2014.07.005.

[9] Li, Q.; Zhang, N.; Yang, Y.; Wang, G.; Ng, D. H. L. High Efficiency Photocatalysis for Pollutant Degradation with MoS_2/C_3N_4 Heterostructures. *Langmuir* **2014**, *30* (29), 8965–8972 DOI: 10.1021/la502033t.

[10] Kang, Y.; Gong, Y.; Hu, Z.; Li, Z.; Qiu, Z.; Zhu, X.; Ajayan, P. M.; Fang, Z. Plasmonic Hot Electron Enhanced MoS_2 Photocatalysis in Hydrogen Evolution. *Nanoscale* **2015**, *7* (10), 4482–4488 DOI: 10.1039/c4nr07303g.

[11] Spalvins, T. A Review of Recent Advances in Solid Film Lubrication. *J. Vac. Sci. Technol. A* **1987**, *5* (2), 212 DOI: 10.1116/1.574106.

[12] Hilton, M. R.; Bauer, R.; Didziulis, S. V.; Dugger, M. T.; Keem, J. M.; Scholhamer, J. Structural and Tribological Studies of MoS_2 Solid Lubricant Films Having Tailored Metal-Multilayer Nanostructures. *Surf. Coat. Technol.* **1992**, *53* (1), 13–23 DOI: 10.1016/0257-8972(92)90099-V.

[13] Chhowalla, M.; Amaratunga, G. A. J. Thin Films of Fullerene-Like MoS_2 Nanoparticles with Ultra-Low Friction and Wear. *Nature* **2000**, *407* (6801), 164–167 DOI: 10.1038/35025020.

[14] Kooyman, P. J.; van Veen, J. A. R. The Detrimental Effect of Exposure to Air on Supported MoS_2. *Catal. Today* **2008**, *130* (1), 135–138 DOI: 10.1016/j.cattod.2007.07.019.

[15] Hensen, E. J. M.; de Beer, V. H. J.; van Veen, J. A. R.; van Santen, R. A. A Refinement on the Notion of Type I and II (Co)MoS Phases in Hydrotreating Catalysts. *Catal. Lett.* **2002**, *84* (1/2), 59–67 DOI: 10.1023/A:1021024617582.

[16] Egorova, M.; Prins, R. The Role of Ni and Co Promoters in the Simultaneous HDS of Dibenzothiophene and HDN of Amines Over Mo/γ-Al_2O_3 Catalysts. *J. Catal.* **2006**, *241* (1), 162–172 DOI: 10.1016/j.jcat.2006.04.011.

[17] Byskov, L. S.; Nørskov, J. K.; Clausen, B. S.; Topsøe, H. DFT Calculations of Unpromoted and Promoted MoS_2-Based Hydrodesulfurization Catalysts. *J. Catal.* **1999**, *187* (1), 109–122 DOI: 10.1006/jcat.1999.2598.

[18] Zandbergen, H.; Kooyman, P. J.; van Langeveld, A. D. Transfer Systems for Insertion of Specimens Into Electron Microscopes Under Controlled Atmospheres; *Electron Microscopy 1998: Proceedings of the 14th International Congress on Electron Microscopy*, Cancun, Mexico, August 31 - September 4, **1998**; Vol. II, 491–492.

[19] van Haandel, L.; Kooyman, P. J.; van Veen, J. A. R.; Weber, T.; Hensen, E. J. M.; Bremmer, G. M. Structure–Activity Correlations in Hydrodesulfurization Reactions Over Ni-Promoted $Mo_xW_{(1-x)}S_2/Al_2O_3$ Catalysts. *ACS Catal*. **2015**, 7276–7287 DOI: 10.1021/acscatal.5b01806.

[20] Weber, T.; Muijsers, J. C.; Van Wolput, J.; Verhagen, C. P. J.; Niemantsverdriet, J. W. Basic Reaction Steps in the Sulfidation of Crystalline MoO_3 To MoS_2, As Studied by X-Ray Photoelectron and Infrared Emission Spectroscopy. *J. Phys. Chem*. **1996**, *100* (33), 14144–14150 DOI: 10.1021/jp961204y.

[21] Alstrup, I.; Chorkendorff, I.; Candia, R.; Clausen, B. S.; Topsøe, H. A Combined X-Ray Photoelectron and Mössbauer Emission Spectroscopy Study of the State of Cobalt in Sulfided, Supported, and Unsupported Co-Mo Catalysts. *J. Catal.* **1982**, *77* (2), 397–409 DOI: 10.1016/0021-9517(82)90181-6.

[22] Gandubert, A. D.; Legens, C.; Guillaume, D.; Rebours, S.; Payen, E. X-Ray Photoelectron Spectroscopy Surface Quantification of Sulfided CoMoP Catalysts – Relation Between Activity and Promoted Sites – Part I: Influence of the Co/Mo Ratio. *Oil Gas Sci. Technol*. **2007**, *62* (1), 79–89 DOI: 10.2516/ogst:2007007.

[23] Hansen, L. P.; Johnson, E.; Ramasse, Q. M.; Kisielowski, C. F.; Brorson, M.; Helveg, S. Electron Microscopy Studies of Structure and Dynamics in MoS_2-Based Hydrodesulfurization Catalysts. *Microsc. Microanal*. **2014**, *20* (S3), 1566–1567 DOI: 10.1017/S1431927614009568.

[24] Jaramillo, T. F.; Jørgensen, K. P.; Bonde, J. L.; Nielsen, J. H.; Horch, S.; Chorkendorff, I. Identification of Active Edge Sites for Electrochemical H_2 Evolution From MoS_2 Nanocatalysts. *Science* **2007**, *317* (5834), 100–102 DOI: 10.1126/science.1141483.

[25] Lauritsen, J. V.; Nyberg, M.; Vang, R. T.; Bollinger, M. V.; Clausen, B. S.; Topsøe, H.; Jacobsen, K. W.; Lægsgaard, E.; Nørskov, J. K.; Besenbacher, F. Chemistry of One-Dimensional Metallic Edge States in MoS_2 Nanoclusters. *Nanotechnology* **2003**, *14* (3), 385–389 DOI: 10.1088/0957-4484/14/3/306.

[26] Hensen, E. J. M.; Kooyman, P. J.; van der Meer, Y.; van der Kraan, A.; de Beer, V. H. J.; van Veen, J. A. R.; van Santen, R. A. The Relation Between Morphology and Hydrotreating Activity for Supported MoS_2 Particles. *J. Catal.* **2001**, *199* (2), 224–235

DOI: 10.1006/jcat.2000.3158.

[27] Temel, B.; Tuxen, A. K.; Kibsgaard, J.; Topsøe, N.-Y.; Hinnemann, B.; Knudsen, K. G.; Topsøe, H.; Lauritsen, J. V. Atomic-Scale Insight Into the Origin of Pyridine Inhibition of MoS_2-Based Hydrotreating Catalysts. *J. Catal*. **2010**, *271* (2), 280–289 DOI: 10.1016/j.jcat.2010.02.007.

[28] Tuxen, A. K.; Kibsgaard, J.; Gøbel, H.; Lægsgaard, E.; Topsøe, H.; Lauritsen, J. V.; Besenbacher, F. Size Threshold in the Dibenzothiophene Adsorption on MoS_2 Nanoclusters. *ACS Nano* **2010**, *4* (8), 4677–4682 DOI: 10.1021/nn1011013.

[29] Lauritsen, J. V. Atomic-Scale Structure of Co–Mo–S Nanoclusters in Hydrotreating Catalysts. *J. Catal*. **2001**, *197* (1), 1–5 DOI: 10.1006/jcat.2000.3088.

[30] Lauritsen, J. V.; Kibsgaard, J.; Olesen, G. H.; Moses, P. G.; Hinnemann, B.; Helveg, S.; Nørskov, J. K.; Clausen, B. S.; Topsøe, H.; Lægsgaard, E.; *et al*. Location and Coordination of Promoter Atoms in Co- and Ni-Promoted MoS_2-Based Hydrotreating Catalysts. *J. Catal.* **2007**, *249* (2), 220–233 DOI: 10.1016/j.jcat.2007.04.013.

[31] Kibsgaard, J.; Tuxen, A. K.; Knudsen, K. G.; Brorson, M.; Topsøe, H.; Lægsgaard, E.; Lauritsen, J. V.; Besenbacher, F. Comparative Atomic-Scale Analysis of Promotional Effects by Late 3d-Transition Metals in MoS_2 Hydrotreating Catalysts. *J. Catal.* **2010**, *272* (2), 195–203 DOI: 10.1016/j.jcat.2010.03.018.

[32] Zhu, Y.; Ramasse, Q. M.; Brorson, M.; Moses, P. G.; Hansen, L. P.; Kisielowski, C. F.; Helveg, S. Visualizing the Stoichiometry of Industrial-Style Co-Mo-S Catalysts with Single-Atom Sensitivity. *Angew. Chem. Int. Ed*. **2014**, *53* (40), 10723–10727 DOI: 10.1002/anie.201405690.

[33] Yoshimura, Y.; Matsubayashi, N.; Yokokawa, H.; Sato, T.; Shimada, H.; Nishijima, A. Temperature-Programmed Oxidation of Sulfided Cobalt-Molybdate/Alumina Catalysts. *Ind. Eng. Chem. Res*. **1991**, *30* (6), 1092–1099 DOI: 10.1021/ie00054a004.

[34] Salmeron, M.; Somorjai, G. A.; Wold, A.; Chianelli, R.; Liang, K. S. The Adsorption and Binding of Thiophene, Butene and H_2S on the Basal Plane of MoS_2 Single Crystals. *Chem. Phys. Lett.* **1982**, *90* (2), 105–107 DOI: 10.1016/0009-2614(82)83620-8.

[35] Kushmerick, J. G.; Weiss, P. S. Mobile Promoters on Anisotropic Catalysts: Nickel on MoS_2; *J. Phys. Chem. B*, **1998**; *102*, 10094–10097 DOI: 10.1021/jp982752.

[36] Zmierczak, W.; Muralidhar, G.; Massoth, F. E. Studies on Molybdena Catalysts XI. Oxygen Chemisorption on Sulfided Catalysts. *J. Catal.* **1982**, *77* (2), 432–438 DOI: 10.1016/0021-9517(82)90184-1.

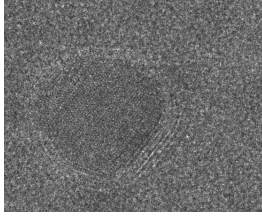


psi
kPa
bar
B
WIKA
Psi
kPa
bar
B
WIKA
KL 2.5
80